Received: 7 December 2024 | Revised: 14 March 2025 | Accepted: 15 April 2025 | Published online: 08 May 2025

RESEARCH ARTICLE

Archives of Advanced Engineering Science
2025, Vol. 00(00) 1–10
DOI: 10.47852/bonviewAAES52024981

BON VIEW PUBLISHING

Strengthening and Toughening Mechanisms of Continuous SiC Fiber-Reinforced TiAl4822/Ti6Al4V Layered Composite Prepared by Hot Pressing

Hongyan Wu[1], Shouyin Zhang[1,*], Kun Zhang[1], Baiping Lu[1] and Zhenjun Wang[1]

[1]*School of Materials Science and Engineering, Nanchang Hangkong University, China*

Abstract: In order to improve the intrinsic brittleness of TiAl4822, Ti6Al4V alloy with outstanding ductility and toughness can be applied as a competitive candidate by constructing the TiAl4822/Ti6Al4V laminated composite. Continuous SiC fibers were introduced into the laminated composite to further enhance the comprehensive performance of the laminated composite. Using SiC fibers, TiAl4822 foil, and Ti6Al4V foil as raw materials, continuous SiC fiber-reinforced TiAl4822/Ti6Al4V layered composite material was fabricated through a vacuum hot-pressing method using the foil-fiber-foil method. A phase-structured interface with a specific sequence was formed between SiC fiber and Ti6Al4V matrix, exhibiting a thickness of 6 μm. A dense bonding interface between TiAl4822 and Ti6Al4V with a thickness of about 80 μm was obtained. No evident cracks or holes were observed at the interface. The resulting SiC fiber-reinforced composite material exhibited superior mechanical properties compared to the traditional TiAl4822/Ti6Al4V layered composite material. Specifically, relative to the unreinforced TiAl4822/Ti6Al4V composite, it had a tensile strength of 727.65 MPa (14.3% improvement), elongation at break of 1.42% (20.3% improvement), elastic modulus of 176 GPa (30.4% improvement), and flexural strength of 1353.6 MPa (21.5% improvement).

Keywords: SiC fiber-reinforced, TiAl4822/Ti6Al4V layered composite, interface evolution, hot pressing

1. Introduction

TiAl-based alloys have great application potential as high-temperature structural materials in aviation, aerospace, automotive, and other industries due to high specific strength, specific stiffness, good creep resistance, and oxidation resistance [1, 2]. However, the low fracture toughness and ductility have greatly restricted the practical utilization of TiAl-based alloys. Researchers have drawn inspiration from natural biological structures such as shell nacre, abalone shell, and animal bones [3, 4], which employ the combination of a strong layer and a tough layer; stacked composites with excellent fracture toughness and high strength were prepared. These composites possess unique performance advantages that make them highly attractive for advanced aerospace applications [5, 6]. By incorporating continuous SiC fibers with excellent properties such as high strength, high modulus, and low density into metal matrix composites based on laminated materials, the high-temperature performance, specific strength, and specific stiffness of the composites are further improved.

The interface of continuous SiC fiber-reinforced metal composites designed with flexible microstructure has the characteristics of multilevel and multi-scale, which significantly improves fatigue resistance and damage tolerance. The interface comprises a nanoscale amorphous carbon layer (2–5 nm) formed during high-temperature processing, a submicron-scale reaction zone (100–500 nm) consisting of TiC and Ti_5Si_3 phases, and a microscale mechanical interlocking structure (1–5 μm) achieved through fiber surface texturing [7]. Yu et al. [8] prepared biomimetic SiC-reinforced Ti-intermetallic layered composites. The tensile strength, flexural strength, and fracture toughness of the composites along the SiC longitudinal direction increased by 53%, 74%, and 75% compared to those without reinforcement of the SiC fibers. Jing et al. [4] prepared Ti-multilayer intermetallic/SiC fiber-reinforced Ti matrix composites using vacuum hot-pressing (VHP) techniques. The tensile strength and flexural strength of the composite in the longitudinal direction of SiC fibers were markedly improved. Zhang et al. [9] investigated the mechanical behaviors and failure mechanisms of SiC fiber-reinforced Ti/Ti2AlNb. Results showed that SiC fiber and ductile metal Ti achieved perfect metallurgical bonding. These findings demonstrate that the introduction of continuous silicon carbide fibers can effectively improve the mechanical properties of composite materials, which are mainly related to the crack deflection of the layered structure and the strengthening of the fiber.

Due to titanium's high chemical reactivity, a strong interface reaction occurs between the fiber and titanium alloy matrix. Interface products will affect the mechanical properties of the composite [10]. For example, the formation of thin and uniform interfacial

***Corresponding author:** Shouyin Zhang, School of Materials Science and Engineering, Nanchang Hangkong University, China. Email: zhangsy@nchu.edu.cn

products (such as TiC, Ti_5Si_3, etc.) through interfacial reactions can enhance the interfacial bonding strength between SiC fibers and the titanium alloy matrix. This improves the efficiency of stress transfer from the matrix to the fibers, thereby increasing the overall strength and stiffness of the composite material. Feng and Yang's study [11] revealed that the interface between SiC fiber and Ti6Al4V was composed of a narrow fine-grained TiC layer close to the SiC fiber and a wider TiC+Ti_5Si_3 mixed layer close to the matrix. The presence of the C coating was found to avoid a direct reaction of the fiber with the matrix. Fellah et al. [12] and Valenza et al. [13] discovered ternary phase Ti_3SiC_2 in their studies. Li and Zhang's research [14] identified that a fine-grain sublayer consisting of TiC+Ti_5Si_3 is located close to SiC fiber within the interface layer, while larger TiC particles are the second reaction layer separated from the ternary phase Ti_3SiC_2. Huang et al. [15] discussed the distribution patterns of interface reaction products and explained the interface generation mechanism according to different interface reactions. The interface reaction between fiber and matrix, the arrangement of fiber, and the toughening mechanism of fiber need to be further studied under different processes.

In contrast to the existing studies on SiC-reinforced composites that focus on a single-matrix material and fabrication process, as well as TiAl4822/Ti6Al4V laminated composites without SiC fiber reinforcement, this paper proposes a method that combines continuous fiber reinforcement with a laminated structure. By utilizing continuous SiC fibers as the reinforcement to enhance Ti6Al4V/TiAl4822 laminated composites, the overall performance of the composite material is further improved. Continuous SiC fiber-reinforced TiAl4822/Ti6Al4V layered composites were fabricated using the foil-fiber-foil approach combined with the VHP method; the microstructure and properties of the composite material were studied. The microstructure of the interface region between SiC fiber and Ti6Al4V was observed and analyzed, with a detailed analysis and summary of the structural evolution at the fiber-matrix interface. The mechanical properties of the composite were assessed through tensile and bending tests. The formation mechanism of the fiber-matrix interface was analyzed by scanning electron microscopy (SEM), transmission electron microscopy (TEM), and other characterization methods. However, due to the limitations of experimental equipment an conditions, the experimental cycle was prolonged, and thus, further mechanical property testing experiments on this composite material could not be conducted.

2. Experimental Procedures

2.1. Structural design

The TiAl4822 alloy utilized in this study was prepared through plasma melting. Ti6Al4V foil (0.5 mm) was produced by multi-pass rolling. The chemical compositions are presented in Table 1. SiC fibers fabricated by the Beijing Institute of Aeronautical Materials were selected as the reinforcing component, providing the lamellar composites with enhanced mechanical properties. The fibers have a diameter of 120 μm, featuring a tungsten core with a diameter of 16 μm and an outer layer of β-SiC (50 μm thick), as depicted in Figure 1. A layer of carbon (2 μm) was coated via chemical vapor deposition to inhibit the interface reactions. The TiAl4822 ingot was sliced into three rectangular layers (100 mm × 50 mm) with a thickness of 630 μm using wire electrical discharge machining. Subsequently, the prepared TiAl4822 layers were ground with sandpaper to eliminate the surface oxide film. Ti6Al4V foils with a thickness of 300 μm and 500 μm were also cut into the dimension of 100 mm × 50 mm. The prepared TiAl4822 layers and Ti6Al4V foils were washed in 10% HF aqueous solution for 90 s, rinsed with alcohol, and ultimately ultrasonically washed in distilled water for 5 min to remove surface impurities.

The fibers were pre-woven in order to avoid fiber segregation. Al foil is not utilized in the preparation of SiC fibers, ensuring that the interface between Ti6Al4V and TiAl4822 is well bonded. This approach prevents contamination of SiC fibers during the weaving process, thereby avoiding the introduction of impurities. During hot pressing, while the TiAl4822 alloy exhibits poor bonding with SiC fibers, it bonds well with Ti6Al4V. Consequently, Ti6Al4V is selected as the matrix material for reinforcing fibers. The fiber weaving process is illustrated in Figure 2. Rectangular

Table 1
Chemical composition of TiAl alloy and Ti6Al4V (wt. %)

Materials	Composition (%)
TiAl4822	Ti: Margin Al 48.1, Cr 1.92, Nb 1.95, Fe < 0.03, C < 0.03, O 0.24, N < 0.03, H 0.04
Ti6Al4V	Ti: Margin Al 5.5–6.8, V 3.5–4.5, Fe < 0.3, C < 0.1, N < 0.05, H < 0.015, O < 0.2

Figure 1
Fracture morphology of SiC fiber

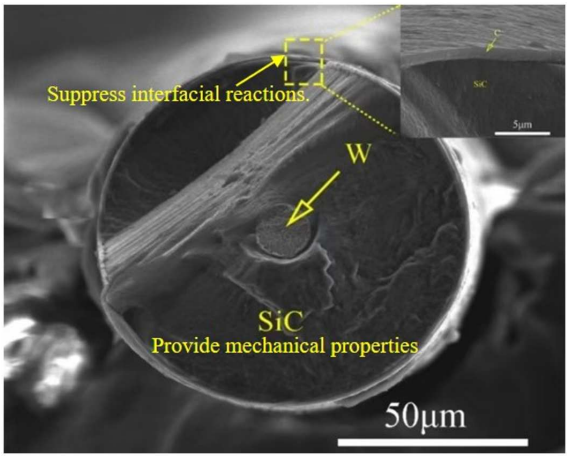

Figure 2
SiC fiber prefabrication process: (a) schematic diagram; (b) fiber cloth

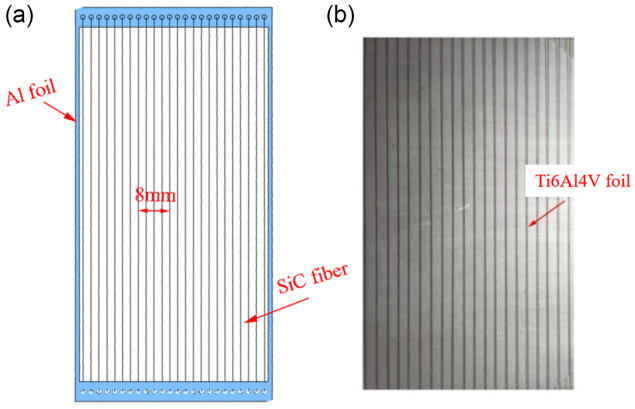

Figure 3
Stack sequence diagram: (a) before hot pressing; (b) after hot pressing

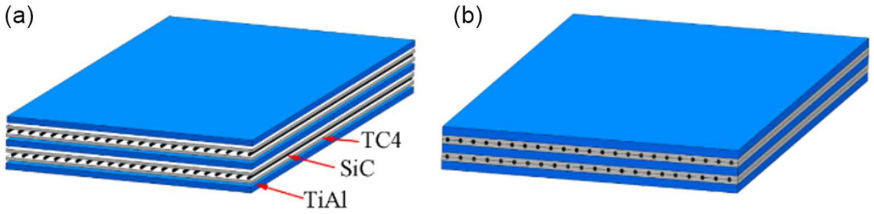

Figure 4
Process parameters of hot pressing

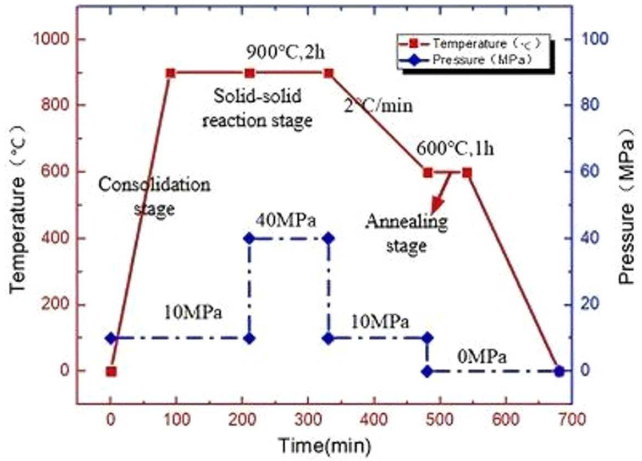

frames (100 mm × 50 mm) were created by cutting aluminum foil, and holes with a spacing of 2 mm were drilled along the short edges of the rectangles. Subsequently, the fibers were woven, as shown in Figure 2(a). The short rectangular edges of the fiber cloth were glued to the Ti6Al4V foil with organic glue to prepare a 2 mm equally spaced fiber cloth, as shown in Figure 2(b). During the hot-pressing process, as the temperature increases, a minimal amount of polyester fiber at both ends undergoes vaporization. This prevents the introduction of impurities while the increment in pressure effectively secures the fiber position and ensures the consistency of fiber spacing.

The experiment was designed with three layers of TiAl4822, each with a thickness of 630 μm, two layers of Ti6Al4V with thicknesses of 300 μm and 500 μm, respectively, and a number of SiC fibers with a diameter of 0.12 mm. The prepared Ti6Al4V foil, TiAl foil, and SiC fiber cloth were sequentially stacked in the order as depicted in Figure 3. A laminated preform with a targeted volume fraction of 45% for the Ti layer was designed.

2.2. Sintering

The laminated preform was placed into a mold, and SiC fiber-reinforced TiAl4822/Ti6Al4V layered composites were fabricated using a vacuum autoclave (ZM-44-12Y). Following the vacuuming process, hot pressing is conducted under a vacuum level exceeding 1.33 × 10^{-3} Pa in order to minimize oxidation. The process parameters of the VHP procedure are illustrated in Figure 4.

The VHP process comprises three stages: the consolidation phase, the solid-solid reaction, and the annealing phase. During the consolidation stage, the temperature was increased from room temperature to 900 °C at a heating rate of 10 °C/min and maintained for 120 min under a pressure of 10 MPa. In the solid-solid reaction stage, a temperature of 900 °C was sustained for 120 min under a pressure of 40 MPa. In the annealing stage, the temperature was reduced to 600 °C and maintained for 60 minutes at that temperature before cooling down in the furnace.

2.3. Material characterization

The prepared continuous SiC fiber-reinforced TiAl4822/Ti6Al4V layered composite was sectioned using an electric spark wire cutter and subsequently embedded in epoxy resin. The specimens were ground with silicon carbide, then polished with a 1.0 μm and 0.5 μm diamond grinding paste, and then subjected to corrosion using a 5% HF+15% HNO_3 aqueous solution for a duration of 10~15 s for the materials studied in this paper. The microstructure of composites was characterized utilizing light microscopy, SEM, energy-dispersive X-ray spectroscopy (EDS), and TEM.

2.4. Mechanical property measurements

The continuous SiC fiber-reinforced TiAl4822/Ti6Al4V layered composites were subjected to a static tensile test at room temperature using the universal testing machine model CMT6103 according to ASTM D3552-96(07), with a loading rate of 0.1 mm/min. The gauge length, width, and thickness of the tensile test specimen are 15 mm, 4 mm, and 3.5 mm, respectively. The constant loading rate of the three-point bending test is 2 mm/min. The dimensions of the bending test specimen are specified as follows: length – 80 mm, width – 15 mm, and thickness – 3.5 mm. The detailed specimen dimensions are shown in Figure 5.

3. Results and Discussion

3.1. Microstructure characterization

Figure 6(a) shows the cross-section of a fabricated SiC fiber-reinforced TiAl4822/Ti6Al4V layered composite, which is spliced

Figure 5
Schematic of the specimens: (a) tensile test; (b) three-point bending test

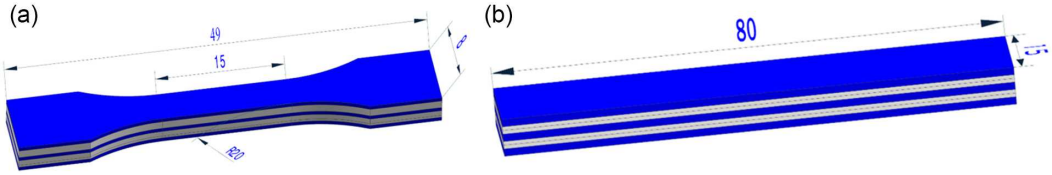

Figure 6
Cross-section of SiC fiber-reinforced TiAl4822/Ti6Al4V: (a) light microscope diagram; (b) schematic diagram

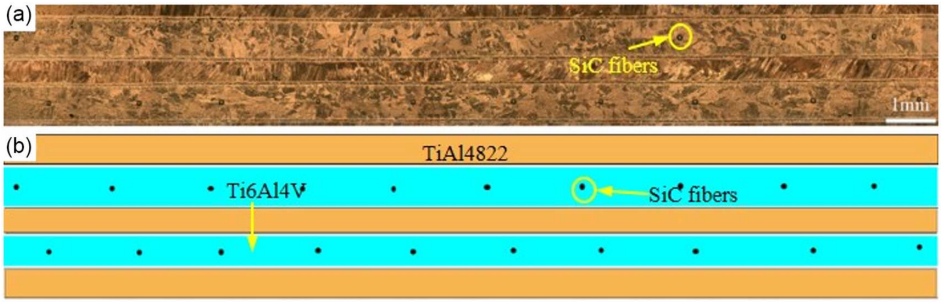

Figure 7
(a) and (b) SiC fiber/Ti6Al4V interface; (c) and (d) TiAl4822/Ti6Al4V interface

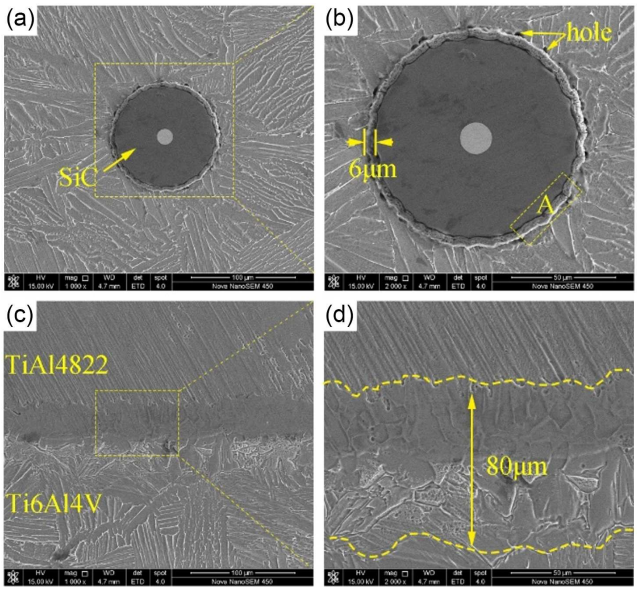

by multiple light microscope diagrams. It can be observed that the SiC fibers are uniformly distributed within the Ti6Al4V matrix, with a fiber spacing of 2 mm. Figure 6(b) presents the schematic diagram consisting of TiAl4822 intermetallic compound (yellow), Ti6Al4V (green), and reinforcement SiC fibers (black dots) distributed in the ductile Ti6Al4V layer.

The microstructures of SiC fiber-reinforced TiAl4822/Ti6Al4V are depicted in Figure 7. As shown in Figure 7(a) and (b), the interface layer thickness between SiC fiber and Ti6Al4V after hot-pressing measures approximately 6 μm. The interface layer between Ti6Al4V and TiAl4822 is shown in Figure 7(c) and (d). The thickness of the interface layer is approximately 80 μm. The intermetallic compounds TiAl4822 and Ti6Al4V were selected as the layered materials. As the experimental time progressed, atomic diffusion gradually stabilized, leading to a consistent atomic diffusion rate. This avoided the issue of interface layer defects caused by the Kirkendall effect during the preparation process [16]. The interface achieved excellent metallurgical bonding, with no significant cracks or voids observed, ensuring strong interfacial bonding strength and thereby contributing to the enhancement of the material's mechanical properties.

Figure 8 shows the XRD pattern of TiAl4822/Ti6Al4V and SiC fiber-reinforced TiAl4822/Ti6Al4V layered composite. The result shows that the layered composites contain α-Ti, β-Ti, α_2-Ti_3Al, Ti_2Al, and γ-TiAl phases. Additionally, in the process of preparing SiC fiber-reinforced TiAl4822/Ti6Al4V layered composite by the VHP method, interfacial reactions have led to the formation of TiC and Ti_5Si_3 at the interface between the SiC fiber and Ti6Al4V matrix. Based on the test results of the mechanical properties in this paper, TiC and Ti_5Si_3 work together to improve the interface bonding strength between SiC fiber and matrix, which is conducive to effective load transfer and stress distribution. Ti_5Si_3 particles can be used as a barrier to crack propagation, promote the crack bridging

Figure 8
XRD pattern of TiAl4822/Ti6Al4V layered composite and SiC fiber-reinforced TiAl4822/Ti6Al4V layered composite: (a) TiAl4822/Ti6Al4V l; (b) SiC fiber-reinforced TiAl4822/Ti6Al4V

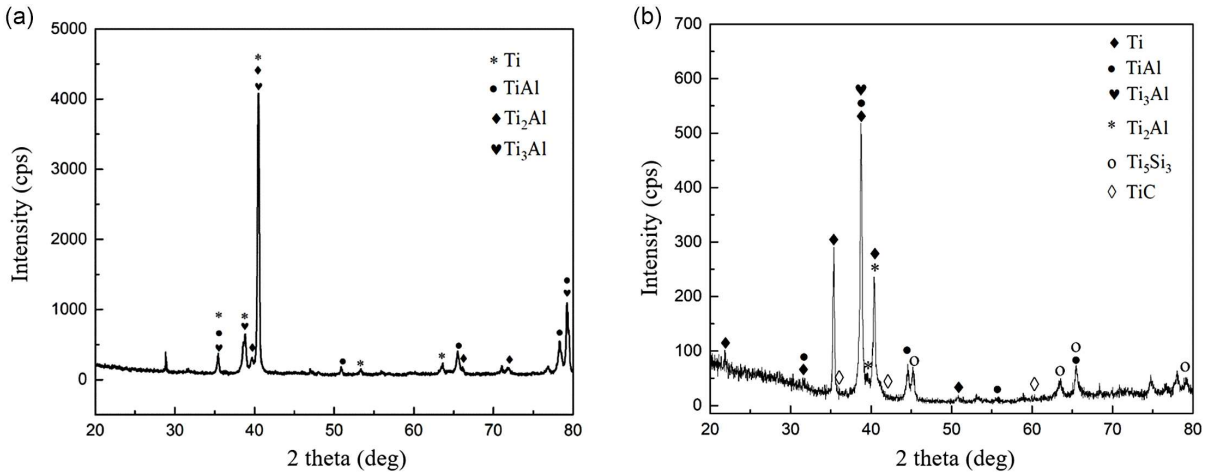

Figure 9
SiC fiber-reinforced TiAl4822/Ti6Al4V layered composite energy spectrum analysis diagram: (a) TiAl4822/Ti6Al4V interface region; (b) and (c) SiC fiber/Ti6Al4V interface region

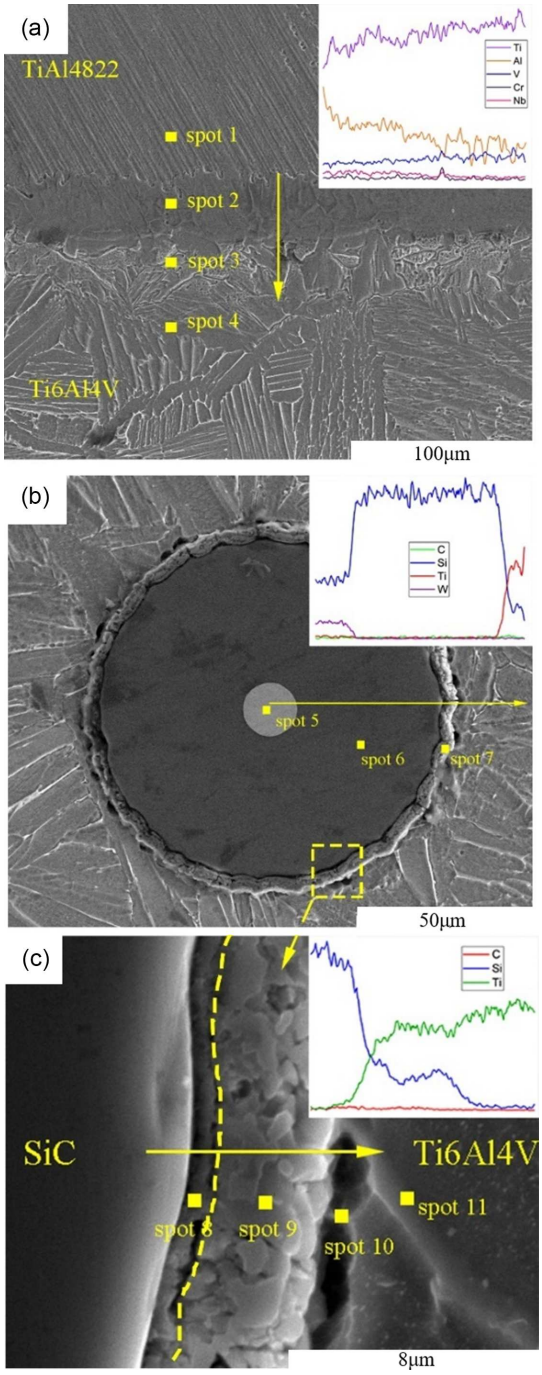

and deflection mechanism, and improve the fracture toughness of composite materials. Moreover, Ti_5Si_3 has excellent thermal stability and oxidation resistance, which contributes to the performance of the composite in high-temperature environments [17].

The energy spectrum analysis of the fiber-reinforced TiAl4822/Ti6Al4V layered composites is illustrated in Figure 9. Based on the phase retrieved in the XRD pattern and the scanning results in Table 2, it can be concluded that point 1~4 correspond to TiAl4822, Ti_2Al, Ti_3Al, and Ti6Al4V phases, respectively. Figure 9(b) and (c) correspond to the energy spectral lines and spot scans of the interface region of SiC fiber and Ti6Al4V matrix. Figure 9(c) presents the

Table 2
Distribution of energy spectrum scanning elements (at %)

Point no.	Al	Ti	Si	C
Spot 1	46.81	48.66		
Spot 2	31.37	65.68		
Spot 3	22.90	72.88		
Spot 4	16.15	81.37		
Spot 5				70.44
Spot 6			45.87	54.05
Spot 7		55.95	28.38	15.66
Spot 8		35.99	27.01	37.00
Spot 9		58.90	25.01	16.10
Spot 10		83.94	6.06	
Spot 11	9.33	89.27	1.40	

enlarged image of the fiber/matrix interface region. The findings indicate that points 5 and 6 represent the W core of the fiber and the SiC matrix, respectively. The distributions of elements obtained from energy spectrum scanning at points 7, 8, and 9 in Figure 9 are presented in Table 2. The results reveal that there are three elements (Ti, Si, and C) distributed at the interface layer between SiC fiber and matrix (point 7). It can be observed that the fiber/matrix interface layer can be divided into a narrow and a wide layer. According to the scan results of points 10 and 11, the right side of the interface layer is the Ti6Al4V matrix.

Figure 10 shows the SiC/Ti6Al4V interface region with high magnification. The interface region consists of two sublayers: a fine-grain layer (with a thickness of 1 μm) close to the SiC fiber and a coarse-grain layer (with a thickness of 5 μm) near the Ti6Al4V matrix. The grain sizes of these two layers are about 0.05 μm and 1 μm, respectively. The EDS surface scan was conducted in the area of the enlarged image. C coating layer at the starting SiC fiber was consumed completely. Element C in the C coating layer and SiC fiber react with the element Ti through diffusion during the hot-pressing process, resulting in a fine-grain layer close to the SiC fiber. From

Figure 10
SiC/Ti6Al4V interface area: (a) high magnification scanning electron microscopy image; (b) EDS surface scan of the interface area

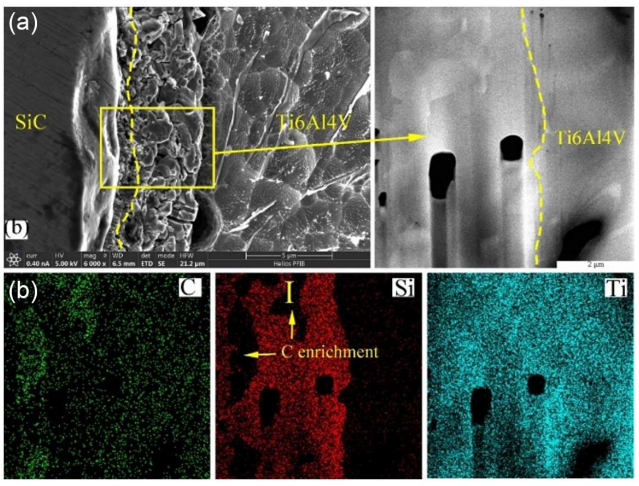

Figure 11
SiC/C/Ti6Al4V composite interface region: (a) TEM bright-field image; (b) phase electron diffraction spots in the interface region; (c) EDS line scan results in the interface layer

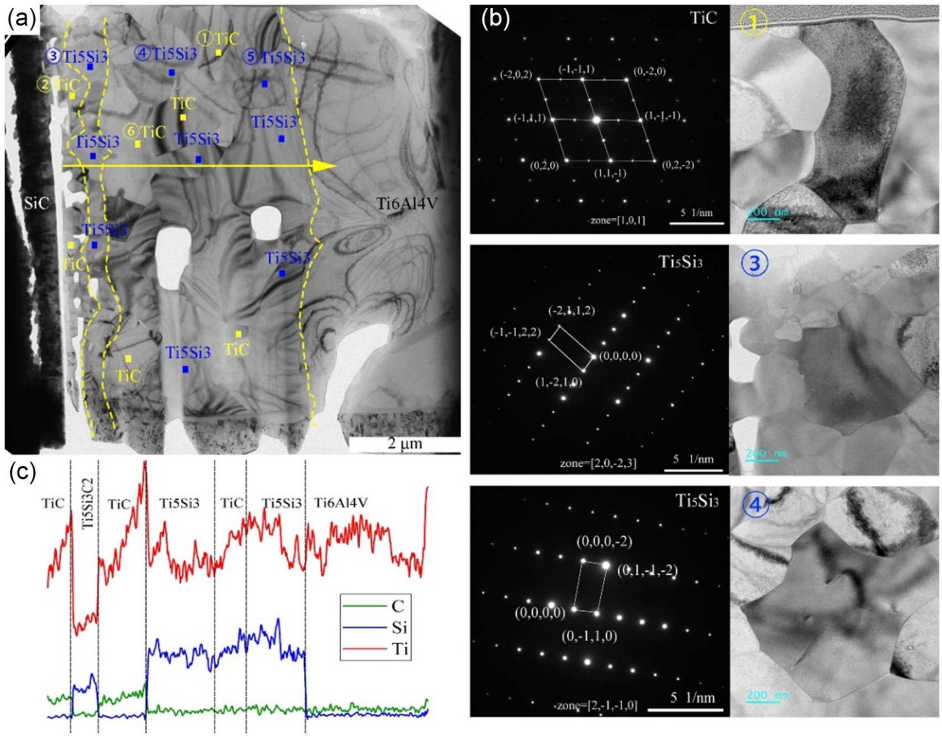

the element distribution of Si and Ti, it can be found that the element Si is mainly distributed in the interface layer area. However, element Ti is uniformly distributed both in the interface layer and the Ti6Al4V matrix.

The content distributions of C and Si in the interface region are found to be complementary, as depicted in Figure 10(b). It is noteworthy that there are enrichment regions of C element near the SiC fiber within the interface region. Additionally, a relatively high Ti content is observed in these C enrichment regions, indicating the possible formation of TiC through reaction. The resultant phases in the enrichment region of Si and Ti include Ti_5Si_3, Ti_5Si_4, and Ti_3Si [15].

The TEM bright-field image and the line scanning results across the SiC/Ti6Al4V interface layer are presented in Figure 11. It can be observed that there is an alternating enrichment of titanium (Ti), silicon (Si), and carbon (C) elements within the interface layer. Combined with the TEM bright-field image and the EDS results, it can be found that the interface layer can be divided into six sublayers.

Point scanning was conducted to analyze the element composition of point 1~6 in the six sublayers, and the results are presented in Table 3. The spot-scanning analysis revealed that the atomic ratio of Ti:Si:C near the SiC fiber (point 3) is approximately 5:3:2. According to previous studies [18–20], the formation temperature of $Ti_5Si_3C_2$ in the solid-solid reaction is higher than 1000 °C. $Ti_5Si_3C_X$ is a solid solution with dissolved C in Ti_5Si_3 [21, 22]. Carbon atoms are dissolved as interstitial atoms at the corner positions within $Ti_5Si_3C_X$ [14]. Since the hot-pressing process temperature employed in this study was set at 900 °C, it can be inferred that Ti_5Si_3 phase with a high concentration of C atoms exists in this region instead of $Ti_5Si_3C_2$. The Ti_5Si_3 sublayer both near Ti6Al4V matrix and in the middle of the interface region contains a small amount of TiC phase.

Table 3
Distribution of elements at points 1, 2, 3, and 4 in Figure 11 (at %)

Point	Ti	Si	C
Spot 1	45.63	0	54.37
Spot 2	44.79	8.21	47.01
Spot 3	50.09	28.28	21.62
Spot 4	64.65	24.77	10.59
Spot 5	60.30	31.25	8.45
Spot 6	52.38	0	47.62

The phase composition of the interface area is marked in Figure 11(a) according to the EDS line scan and point scan results. The interface layer can be divided into three TiC+Ti_5Si_3 layers, as shown in Figure 11(c). The phase distribution within the SiC/Ti6Al4V interface region follows a sequence of SiC ‖ TiC ‖ Ti_5Si_3 ‖ TiC ‖ Ti_5Si_3 ‖ TiC ‖ Ti_5Si_3 ‖Ti6Al4V. Electron diffraction spots corresponding to regions 1, 3, and 4 within the interface region are illustrated in Figure 11(b).

At the initiation of the reaction, titanium from Ti6Al4V diffused toward the C coating. The resulting reaction yielded fine-grain TiC proximity to SiC fiber and coarse-grain TiC near the Ti6Al4V matrix. When the C coating was consumed completely, the interfacial reaction penetrated into the SiC fiber. The diffusion rate of C atoms exceeded than Si atoms due to their smaller diameter. Consequently, the C element in the fiber took the lead in diffusing to the original interfacial reaction zone and then reacted with the highly active Ti that diffused across the interfacial layer. TiC particles were formed preferentially near the SiC fiber. Because of the high nucleation rate of TiC on SiC fiber, fine TiC grains near SiC fibers were obtained. Si atoms diffused to the matrix across the generated layer and then reacted with Ti to form Ti_5Si_3 particles. As diffusion pro-

Figure 12
TiAl4822/Ti6Al4V and SiC fiber-reinforced TiAl4822/Ti6Al4V layered composites: (a) room temperature tensile stress-strain curve; (b) bending displacement-load curve

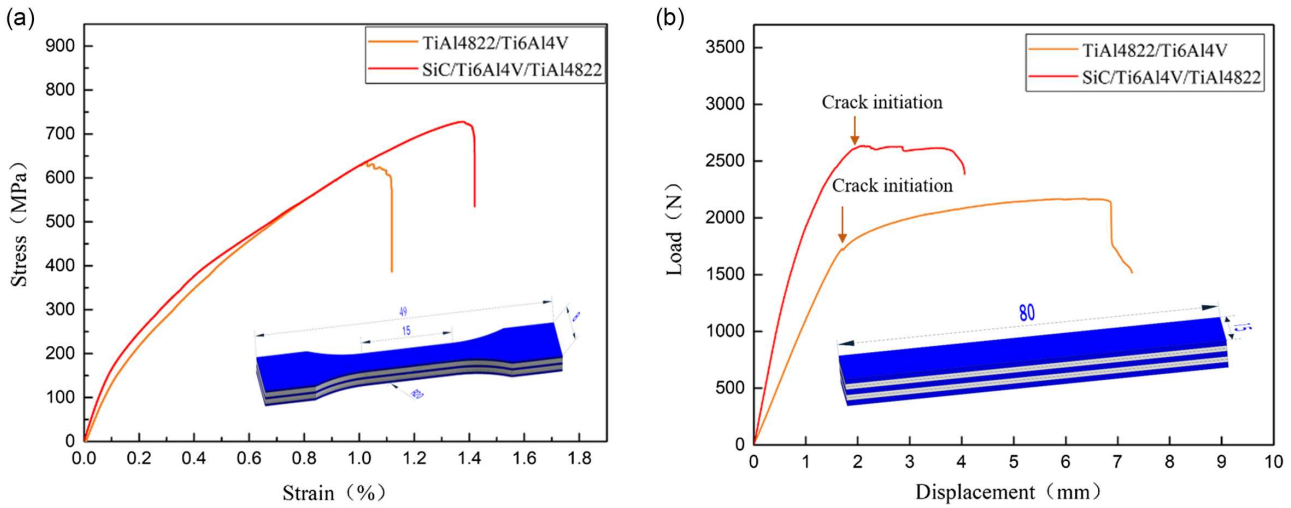

Table 4
TiAl4822/Ti6Al4V and SiC fiber-reinforced TiAl4822/Ti6Al4V layered composites

Materials	Tensile strength (MPa)	Elongation (%)	Elastic modulus (GPa)	Flexural strength (MPa)
TiAl4822/Ti6Al4V	636.9	1.13	135	1114.1
SiC/Ti6Al4V /TiAl4822	727.65	1.42	176	1353.6

ceeded, TiC and Ti_5Si_3 were saturated by C and Si. With the C and Si atoms diffusing to the matrix across the interface layer continuously, the alternating sublayers of TiC and Ti_5Si_3 are formed. The diffusion of Si atoms resulted in the coarsening of the Ti_5Si_3 particles close to the Ti6Al4V matrix, resulting in the formation of a coarse-grain layer, as illustrated in Figure 10(a).

3.2. Mechanical properties

Figure 12 shows the tensile stress-strain curve and bending load-displacement curve of TiAl4822/Ti6Al4V layered composites with and without SiC fiber reinforcement. The mechanical properties of TiAl4822/Ti6Al4V and SiC fiber-reinforced TiAl4822/Ti6Al4V layered composites are shown in Table 4. The tensile strength of the Ti6Al4V/TiAl4822 layered composite is 636.9 MPa, with an elongation of 1.13%, an elastic modulus of 135 GPa, and a flexural strength of 1114.1 MPa. The tensile strength of the SiC fiber-reinforced Ti6Al4V/TiAl4822 layered composite is 727.65 MPa, with a tensile strain of 1.42%, an elastic modulus of 176 GPa, and a flexural strength of 1353.6 MPa. The tensile strength increases by 4.3% to 727.65 MPa when SiC fibers are introduced, while the tensile strain rises by 20.3% to reach a value of 1.42%. Moreover, the flexural strength reaches 1353.60 MPa in the SiC fiber-reinforced TiAl4822/Ti6Al4V layered composite, exhibiting a remarkable improvement of 21.5% over the TiAl4822/Ti6Al4V layered composite. It is evident that the incorporation of SiC fibers enhances the tensile strength, elongation, and flexural strength of the TiAl4822/Ti6Al4V layered composite compared to its counterpart without fiber reinforcement. The composite material is an ideal candidate for high-temperature components, such as aeroengine blades and spacecraft structures, and has broad application prospects in high-temperature environments such as gas turbines and nuclear reactors.

3.3. Fracture morphology

The tensile fracture morphologies of SiC fiber-reinforced TiAl4822/Ti6Al4V layered composite are depicted in Figure 13.

Figure 13
Macroscopic tensile fracture morphology of SiC fiber-reinforced TiAl4822/Ti6Al4V layered composites

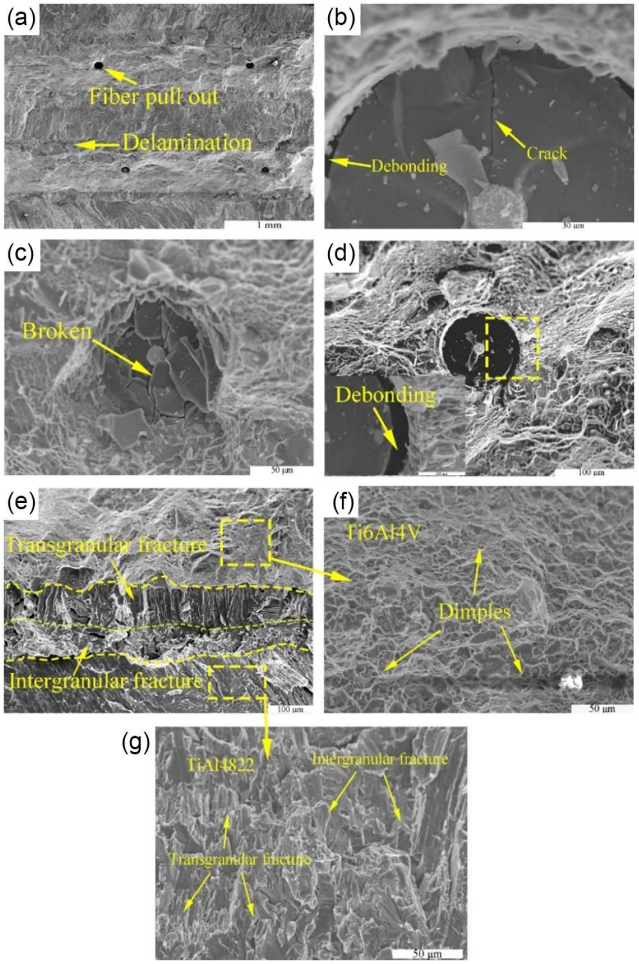

No evident interface delamination is observed, indicating excellent bonding between the Ti6Al4V and TiAl4822 matrices. Figure 13(a) exhibits the orderly arrangement of SiC fibers on the fracture surface, with fiber pull-out suggesting weak bonding strength at the interface between the fiber and Ti6Al4V matrix. When the load applied on the matrix transferred to the SiC fibers and exceeded the longitudinal shear force at the interface with Ti6Al4V, the phenomenon of SiC fiber pulling out occurred. Previous studies [23, 24] have indicated that a too weak fiber/matrix binding interface restricts effective reinforcement by SiC fiber. There are energy absorption phenomena such as fiber debonding, fiber fragmentation, and fiber fracture (Figure 13(b–d)), which contribute to enhancing toughness and strengthening of these composite materials.

The fracture morphologies of the matrices and their interface are depicted in Figure 13(e–g). There are a large number of dimples in the Ti6Al4V matrix, presenting ductile fractures. In Figure 13(g), the fracture surface of the TiAl4822 matrix displays river patterns, which correspond to the typical brittle cleavage fracture. Both ductile fractures and brittle cleavage fractures can be observed in the interface region between the Ti6Al4V and TiAl4822 matrices. During brittle fracture, SiC fibers can redistribute localized stresses, reduce stress concentration, and delay the overall failure of the material. During ductile fracture, the material absorbs a significant amount of energy through plastic deformation, thereby enhancing the toughness of the composite. The laminated structure of TiAl4822/Ti6Al4V effectively prevents the propagation of cleavage cracks, confining them to localized regions and avoiding the overall failure of the material. These fracture mechanisms work together to optimize crack propagation behavior, improve energy absorption capacity, and achieve uniform stress distribution, resulting in outstanding performance of the composite material in terms of strength, toughness, and fracture resistance. Thus, it can be concluded that the introduction of SiC fiber effectively enhances the tensile properties of the composite.

The macroscopic fracture diagrams of the three-point bending test specimen are illustrated in Figure 14. Figure 15 shows the fracture morphologies of the SiC fiber-reinforced TiAl4822/Ti6Al4V layered composite. During the loading process, the bottom layer of the specimen was subjected to the compressive stress, while the top outmost layer was subjected to the tensile stress. As the bending load increased, brittle fracture failure occurred at the outmost TiAl4822 layer on the top layer first, leading to the formation of the main crack. It can be observed that the main crack exhibited deflection at the interface region, presenting zigzag morphologies. Additionally, SiC fiber bending and fracture occurred in the Ti6Al4V layer, and then the crack continued to expand to the middle layer TiAl4822. Various mechanisms such as crack deflection, crack blunting, and crack bridging, as well as secondary cracks and microcracks, were observed during this crack propagation process. These crack propagation mechanisms increase the crack propagation path, effectively absorb external loads, and enhance energy dissipation pathways, ensuring the reliability of the composite materials and improving the load-bearing capacity of SiC fiber-reinforced Ti6Al4V/TiAl4822 layered composites.

Figure 14
Macroscopic fracture diagram of the bending test specimen

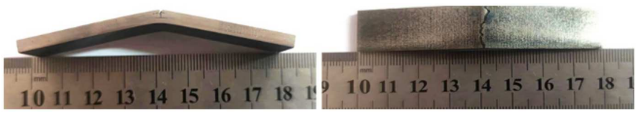

4. Conclusions

Different from the single-matrix and preparation process of traditional composites, the SiC fiber-reinforced TiAl4822/Ti6Al4V layered composites were prepared by the VHP method in this paper. The microstructure and properties of the composites were studied. The main conclusions are as follows:

1) High-quality metallurgical bond interface layers consisting of α_2-Ti_3Al and Ti_2Al with a thickness of about 80 μm were formed between Ti6Al4V and TiAl4822 matrices. By using pre-woven fiber cloth, evenly distributed SiC fibers were introduced into the TiAl4822/Ti6Al4V layered composites. Existing research has primarily focused on single-matrix materials, such as Ti6Al4V or TiAl alloys. However, combining TiAl4822 and Ti6Al4V to form a layered structure represents an innovative

Figure 15
Morphology of SiC fiber-reinforced TiAl4822/Ti6Al4V layered composites

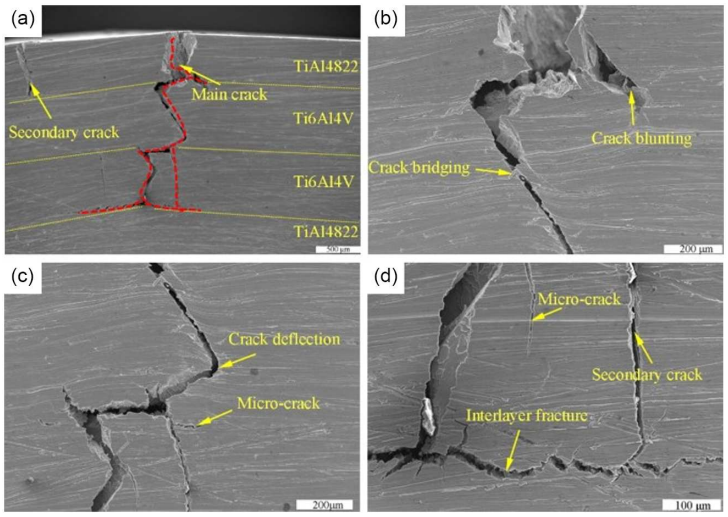

design. This design integrates the high-temperature performance of TiAl4822 with the toughness of Ti6Al4V, achieving complementary properties.

2) The interface layer between SiC fiber/Ti6Al4V can be divided into a fine-grain narrowband adjacent to the SiC fiber and a coarse-grain sublayer close to the matrix. The fine-grain narrowband is the TiC + Ti_5Si_3 layer, which is composed of a thin layer of TiC with small particles and a thick layer of Ti_5Si_3 with coarse particles; the grain sizes were 0.05 μm and 1 μm. The coarse-grain sublayer is composed of two TiC + Ti_5Si_3 layers with larger grain sizes. The phase distribution across the interface layer is SiC || TiC || Ti_5Si_3 || TiC || Ti_5Si_3 || TiC || Ti_5Si_3 || Ti6Al4V. This phase distribution sequence can significantly improve the interfacial bonding strength, toughness, and high-temperature properties of composites through gradient interfacial structure, multi-scale toughening mechanism, and interfacial reaction regulation, which has important scientific significance and engineering value.
3) Compared to traditional single-matrix materials or TiAl4822 /Ti6Al4V laminated composites without SiC fiber reinforcement, the SiC fiber-reinforced TiAl4822/Ti6Al4V laminated composites exhibit significant improvements in both strength and toughness. The SiC fiber-reinforced TiAl4822/Ti6Al4V layered composite exhibits a tensile strength of 727.65 MPa and a tensile strain of 1.42%, with an elastic modulus of 176 GPa. Compared with TiAl4822/Ti6Al4V layered composite, the introduction of SiC fibers significantly enhances the overall performance due to energy-absorbing mechanisms such as fiber/matrix interface debonding, fiber pulling out, and fiber embrittlement during tensile fracture.
4) The flexural strength of SiC fiber-reinforced TiAl4822/Ti6Al4V layered composite was measured to be 1353.6 MPa, exhibiting a significant improvement of 21.5% compared to that of the TiAl4822/Ti6Al4V layered composite. This enhancement can be attributed to the strengthening effect of SiC fibers and the crack deflection ability of the layered structure of lamellar composites. The failure process was accompanied by various energy-dissipating mechanisms, including crack deflection, crack bridging, and interlayer cracking, as well as secondary cracks and microcracks.
5) Most of the existing studies focus on a single interface reaction layer, but this study realizes the overall improvement of interface performance through multilevel and multi-scale interface design. The improvement in overall performance will make this layered composite material an ideal candidate for high-temperature components such as aeroengine blades and spacecraft structural parts. In addition, this composite material has broad application prospects in high-temperature environments such as gas turbines and nuclear reactors.

Funding Support

This study is partially supported by the Jiangxi Provincial Department of Science and Technology (No. 20225BCJ22002).

Ethical Statement

This study does not contain any studies with human or animal subjects performed by any of the authors.

Conflicts of Interest

The authors declare that they have no conflicts of interest to this work.

Data Availability Statement

Data available on request from the corresponding author upon reasonable request.

Author Contribution Statement

Hongyan Wu: Writing – original draft. **Shouyin Zhang:** Conceptualization, Investigation, Resources, Data curation, Writing – review & editing. **Kun Zhang:** Methodology, Formal analysis, Writing – original draft. **Baiping Lu:** Supervision. **Zhenjun Wang:** Visualization, Funding acquisition.

References

[1] Dong, S., Liu, S., Ji, M., Qu, Y., Chen, R., & Guo, J. (2024). Anomalous increase of fracture toughness of TiAl-based alloys at high temperature. *Materials Characterization*, *215*, 114215. https://doi.org/10.1016/j.matchar.2024.114215

[2] Hou, C., Zhang, S., Ma, Z., Lu, B., & Wang, Z. (2021). Effects of SiC fibers and laminated structure on mechanical properties of Ti–Al laminated composites. *Materials*, *14*(6), 1323. https://doi.org/10.3390/ma14061323

[3] Madhav, D., Buffel, B., Moldenaers, P., Desplentere, F., & Vandeginste, V. (2023). A review of nacre-inspired materials: Chemistry, strengthening-deformation mechanism, synthesis, and applications. *Progress in Materials Science*, *139*, 101168. https://doi.org/10.1016/j.pmatsci.2023.101168

[4] Jing, D., Meng, L., Xu, J., Ya, B., Zhao, J., Zhou, B., & Zhang, X. (2023). Microstructure and mechanical properties of highly biomimetic brick-and-mortar structure Ti6Al4V/Al3Ti metal-intermetallic laminate composite. *Materials & Design*, *233*, 112195. https://doi.org/10.1016/j.matdes.2023.112195

[5] Wang, Z., Zhang, X., Liu, M., Zhou, Y., Zha, Z., Li, C., ... & Jiang, F. (2023). Microstructure characterization and mechanical properties of the 304SS-(NiTif/FeAl) metal-intermetallic laminate composites. *Journal of Alloys and Compounds*, *943*, 169117. https://doi.org/10.1016/j.jallcom.2023.169117

[6] Zhang, B., Han, Q., Zhang, J., Han, Z., Niu, S., & Ren, L. (2020). Advanced bio-inspired structural materials: Local properties determine overall performance. *Materials Today*, *41*, 177–199. https://doi.org/10.1016/j.mattod.2020.04.009

[7] Gan, Z., Wang, Y., Zhang, X., Yang, L., Jia, Q., Kong, X., ... & Yang, R. (2024). Microstructure evolution of interface and matrix during the preparation of SiCf/Ti60 composites. *Materials Characterization*, *214*, 114111. https://doi.org/10.1016/j.matchar.2024.114111

[8] Yu, W., Zhu, K., Aman, Y., Guo, Z., & Xiong, S. (2016). Bio-inspired design of SiC f-reinforced multi-layered Ti-intermetallic composite. *Materials & Design*, *101*, 102–108. https://doi.org/10.1016/j.matdes.2016.03.138

[9] Zhang, G., Yuan, M., Li, S., Hou, H., Qu, H., & Zhao, B. (2017). Fabrication and interface reaction of SiC fiber reinforced Ti/Ti2AlNb laminated composite. *Chinese Journal of Rare Metals*, *41*, 1093–1098. https://doi.org/10.13373/j.cnki.cjrm.XY16060004

[10] Lin, C., Wang, S., Yan, H., Han, Y., Zhu, J., & Shi, H. (2021). Optimization mechanisms of microstructure and mechanical

properties of SiC fiber reinforced Ti/Al 3 Ti laminated composite synthesized using titanium barrier. *Metals and Materials International*, *27*, 306–318. https://link.springer.com/article/10.1007/s12540-020-00724-7

[11] Feng, G., & Yang, Y. (2021). Improvement of interfacial compatibility of SiCf/Ti-6Al-4V composites by applying fiber coating and heat treatment. *Materials & Design*, *210*, 110042. https://doi.org/10.1016/j.matdes.2021.110042

[12] Fellah, C., Braun, J., Sauder, C., Sirotti, F., & Berger, M. H. (2020). Influence of the carbon interface on the mechanical behavior of SiC/SiC composites. *Composites Part A: Applied Science and Manufacturing*, *133*, 105867. https://doi.org/10.1016/j.compositesa.2020.105867

[13] Valenza, F., Gambaro, S., Muolo, M. L., Salvo, M., & Casalegno, V. (2018). Wetting of SiC by Al-Ti alloys and joining by in-situ formation of interfacial Ti3Si (Al) C2. *Journal of the European Ceramic Society*, *38*(11), 3727–3734. https://doi.org/10.1016/j.jeurceramsoc.2018.04.025

[14] Li, X., & Zhang, W. (2021). Interfacial reaction in SiCf/C/TiAl matrix composites. *Journal of Materials Research and Technology*, *12*, 1227–1234. https://doi.org/10.1016/j.jmrt.2021.03.072

[15] Huang, B., Li, M., Chen, Y., Luo, X., & Yang, Y. (2015). Interfacial reaction in SiCf/Ti-6Al-4V composite by using transmission electron microscopy. *Materials Characterization*, *109*, 206–215. https://doi.org/10.1016/j.matchar.2015.09.023

[16] Zou, Y., Sun, Z., Tada, S., & Hashimoto, H. (2008). Effect of Al addition on low-temperature synthesis of Ti3SiC2 powder. *Journal of Alloys and Compounds*, *461*(1–2), 579–584. https://doi.org/10.1016/j.jallcom.2007.07.090

[17] Zhang, F., Zhang, B., Chen, X., Zhang, X., Zhu, X., & Du, H. (2020). Computational simulation of voids formation and evolution in Kirkendall effect. *Physica A: Statistical Mechanics and its Applications*, *554*, 124285. https://doi.org/10.1016/j.physa.2020.124285

[18] Zhuo, L., Ji, K., Lu, J., Sun, J., Huo, W., Shao, H., ... & Zhao, Y. (2023). Microstructure characterization and tensile performance of a high-strength titanium alloy with in-situ precipitates of Ti5Si3. *Journal of Alloys and Compounds*, *968*, 171867. https://doi.org/10.1016/j.jallcom.2023.171867

[19] Pourebrahim, A., Baharvandi, H., Foratirad, H., & Ehsani, N. (2019). Low temperature synthesis of high-purity Ti3SiC2 via additional Si through spark plasma sintering. *Journal of Alloys and Compounds*, *789*, 313–322. https://doi.org/10.1016/j.jallcom.2019.03.062

[20] He, G., Xu, J., Zhang, Z., Qian, Y., Zuo, J., Li, M., & Liu, C. (2021). Interfacial reactions and mechanical properties of SiC fiber reinforced Ti3SiC2 and Ti3 (SiAl) C2 composites. *Materials Science and Engineering: A*, *827*, 142069. https://doi.org/10.1016/j.msea.2021.142069

[21] Williams, J. J. (1999). *Structure and high-temperature properties of Ti5Si3 with interstitial additions*. Ames, Iowa: Iowa State University. https://doi.org/10.31274/rtd-180813-13762

[22] Marchin, N., & Ashrafizadeh, F. (2019). Surface structural characterization of TiSiN and TiSiCN coatings produced by cathodic arc physical vapor deposition. *Journal of Surface Science and Engineering*, *15*(39), 47–58. https://sid.ir/paper/400314/fa

[23] Han, Y., Que, Q., Cheng, R., Lin, C., Han, W., Wang, E., ... & Yan, H. (2021). Microstructure evolution and mechanical performances of SiC_f reinforced (Al_3 Ti+ Al_3 Ni)-based metallic–intermetallic laminate composite. *Metals and Materials International*, *27*, 4035. https://link.springer.com/article/10.1007/s12540-020-00942-z

[24] Moslemi, M., Razavi, M., & Zakeri, M. (2024). Effect of the carbon fiber volume fraction on the mechanical properties of SiC matrix composites prepared by spark plasma sintering. *MRS Advances*, *9*, 1150. https://link.springer.com/article/10.1557/s43580-024-00955-5

How to Cite: Wu, H., Zhang, S., Zhang, K., Lu, B., & Wang, Z. (2025). Strengthening and Toughening Mechanisms of Continuous SiC Fiber-Reinforced TiAl4822/Ti6Al4V Layered Composite Prepared by Hot Pressing. *Archives of Advanced Engineering Science*. https://doi.org/10.47852/bonviewAAES52024981